Combining fluorescence fluctuations and photobleaching to quantify surface density

Julius Sefkow-Werner, Elisa Migliorini, Catherine Picart, Dwiria Wahyuni, Irène Wang, Antoine Delon

Combining fluorescence fluctuations and photobleaching to quantify surface density

Julius Sefkow-Werner,[†,¶] Elisa Migliorini,[*,†] Catherine Picart,[†] Dwiria Wahyuni,[‡,§] Irène Wang,[‡] and Antoine Delon[*,‡]

† *BRM ERL 5000 CEA/CNRS/UGA,France*

‡ *LIPHY, Université Grenoble Alpes and CNRS, F-38000 Grenoble, France*

¶ *LMGP UMR 5628, Grenoble,France*

§ *Current address: Tanjungpura University, Pontianak, Indonesia*

E-mail: Elisa.migliorini@cea.fr; antoine.delon@univ-grenoble-alpes.fr

Abstract

We establish a method, called *pbFFS* for *photobleaching Fluctuation Fluorescence Spectroscopy*, which aims at characterizing molecules or particles labelled with a unknown distribution or fluorophores. Using photobleaching as a control parameter, pbFFS provides information on the distribution of labels and a more reliable estimation of the absolute density or concentration of these molecules. We present a complete theoretical derivation of the pbFFS approach and experimentally apply it to measure the surface density of a monolayer of fluorescently tagged streptavidin molecules that can be used as a base platform for biomimetic systems. The surface density measured by pbFFS is consistent with the results of more standard surface techniques, such as ellipsometry. Compared to those techniques, pbFFS has two main advantages: it enables *in situ* characterization (no dedicated substrates are required) and is applicable to low masses of adsorbed molecules, as demonstrated here by quantifying the density

of biotin-Atto molecules that bind to the streptavidin layer. Besides molecules immobilized on surfaces, we also applied pbFFS to molecules diffusing in solution, to confirm the distribution of labels found on surfaces. Hence, pbFFS provides a set of tools to investigate molecules attached to a variable number of fluorophores, with the aim to quantify either the number of molecules or the distribution of fluorophores, the latter case being especially relevant for oligomerization studies.

Introduction

Biomimetic approaches are popular in medical applications and cellular studies. As the extracellular matrix (ECM) plays a complex role on cell response to drugs, growth factors and morphological cues,[1] it is advantageous to design surfaces mimicking the natural environment of cells in the body for enhancing the efficiency of biomedical products. Moreover these biomaterials can bring a deeper understanding of the influence of selected components of the ECM on cellular processes such as proliferation, migration and differentiation.[2] Developing these biomaterials requires a precise control of the immobilized compounds. Standard surface techniques include spectroscopic ellipsometry and quartz crystal microbalance with dissipation monitoring (QCM-D).[3] However, these techniques are *ex situ* since the surfaces have to be built on auxiliary substrates, which may affect the functionalization process. Moreover, low masses of adsorbed molecules cannot be detected by the above techniques. Fluorescence-based methods would, in principle, allow *in situ* characterization, as well as detection of small surface densities of adsorbed molecules.

Using fluorescently-labelled molecules, a simple image provides relative information on molecular density through its intensity, but estimating the absolute value of the number of molecules requires additional and fragile calibrations.[4] There are alternative approaches based on single molecules strategies, but they are adapted only for very small surface densities.[5] On the other hand, Fluorescence Fluctuation Spectroscopy (FFS) techniques,[6] and more specifically Image Correlation Spectroscopy (ICS) which is suited to the characteriza-

tion of immobile molecules, are intended for absolute quantification. These methods derive historically from Fluorescence Correlation Spectroscopy (FCS) and are based on the notion that signal originating from a confined region within the sample, corresponding to the Point Spread Function (PSF) of the microscope, exhibits statistical fluctuations, since this PSF region does not always include the same number of molecules. The relative amplitude of these fluctuations provides an estimation of the average number of molecules in the PSF region and hence the concentration or density. Molecules cross the PSF either by spontaneous motion, as in the case of FCS, or by scanning the excitation laser (as in confocal microscopy), as in the case of ICS. ICS has been used to assess oligomerization,[7] or qualitatively detect the presence of aggregates through an increase of brightness or a corresponding decrease of number density.[8,9]

In fact, standard FFS techniques can only provide reliable quantitative information if all molecules have the same brightness (or if the distribution of brightness is known). Yet commercially available large proteins are rarely all labelled with the same number of fluorophores, so that they present a distribution of brightness. In this case, the number density of fluorescent entities (molecules or particles) estimated by conventional FFS is underestimated: indeed, part of the measured fluctuations would be due to variations in brightness and not only in number of entities, as usually assumed in FFS. More precisely, if the brightness distribution is characterized by a mean value, $\bar{\epsilon}$ and a standard deviation, σ_ϵ, it can be shown (following[8,10]) that the mean number of entities in the PSF volume or area, as measured by FFS, is related to the true number of entities, N, by:

$$N_{FFS} = \frac{N}{1 + (\sigma_\epsilon/\bar{\epsilon})^2} \tag{1}$$

Consequently, the wider the brightness distribution and the more pronounced is the underestimation of the number density. The same bias affects the estimation of average brightness values (which tend to be overestimated). Using only standard FFS methods, there is no way

to evaluate this bias.

The present work aims at using photobleaching as a control parameter to measure accurately the density of surfaces coated with multiply-labelled entities. The combination of FFS and photobleaching has been proposed previously and used to estimate the degree of labelling,[11] the size of oligomers[12,13] or the surface density of molecules.[14] However the proposed methods were either limited to the specific case of a Poisson distribution of brightness,[11,14] or failed to decipher the real parameters that could be deduced from the photobleaching decay.[12,13]

We present here a complete theoretical description of a method combining ICS to photobleaching, which is not specific to ICS and can be extended to other FFS techniques (for instance FCS, as in[11]): we name it *pbFFS* for *photobleaching FFS*. Compared to previous work, we present a more in-depth theoretical derivation. We show that the measured brightness always decays linearly with photobleaching, whatever the distribution of labels, and hence exactly two outputs can be extracted from this decay: the brightness of a single label and a factor depending on the mean and variance of the number of labels per entity. We stress the fact that the presented method has the advantage to be *calibration free*. Indeed, the standard way to estimate the number of molecules or particles is based on a ratiometric comparison of fluorescence intensity to known standards, while the pbFFS method is self-calibrated.

The pbFFS method is experimentally validated on substrates covered with monolayers of streptavidin molecules via a linker, used as a platform to build biomimetic surfaces step by step by adsorbing biotinylated molecules on top of it.[3,15] We applied pbFFS to streptavidin, fluorescently tagged with Alexa (SAv-Alex). Thanks to an additional assumption about the labelling, we could bracket the mean number of labels per SAv molecule and, hence, estimate the absolute number density of SAv molecules covering the substrate. The resulting densities have been validated by independent QCM-D and ellipsometry measurements. We show that pbFFS is capable of measuring SAv surface densities that span over two orders of magnitude.

Then, pbFFS was used to quantify the number of biotinylated fluorescent molecules (Atto-labelled biotin, bAtto) that attach to a streptavidin base layer. In this case, the mass of adsorbed molecules was too low to be measured with accuracy by QCM-D or ellipsometry (since the mass of bAtto is only 1 kDa as compared to SAv which is 55 kDa). Interestingly, we also found by performing control photobleaching-FCS experiments that bAtto molecules are prone to aggregation in solutions, which potentially impacts the way they bind to the SAv base layer.

Theory

A pbFFS experiment consists in alternating measurement phases, where the fluorescence signal, F, and the mean number of entities, N_{FFS}, (hence the brightness B_{FFS}) are measured, and photobleaching phases, where a higher laser power is sent into the sample to bleach a fraction of the fluorescent labels (or fluorophores) borne by the entities (e.g. Alexa SAv-Alex). The mean number of entities in the Point Spread Function (PSF) region, N_{FFS}, is determined by the inverse of the autocorrelation amplitude as illustrated in Fig. 1. As more fluorophores are photobleached, the image intensity (in ICS) or the photon count rate (in FCS) decreases, while the autocorrelation amplitude increases, denoting a reduction of the number of entities N_{FFS}.

In the following, we derive the rigorous expression of the brightness B_{FFS} as a function of the photobleaching stage (defined as the fraction of remaining fluorescence signal), assuming all fluorophores are independent and have an equal probability to bleach. Although we present the formalism of pbFFS for two-dimensional ICS, the same results apply to three dimensions (solution) and temporal techniques, *e.g.* FCS.

Let us consider $F(x, y)$ the fluorescence signal at pixel x, y. The fluorescence fluctuations, defined as $\delta F(x, y) = F(x, y) - \langle F(x, y) \rangle$ (where the averaging is performed over the image

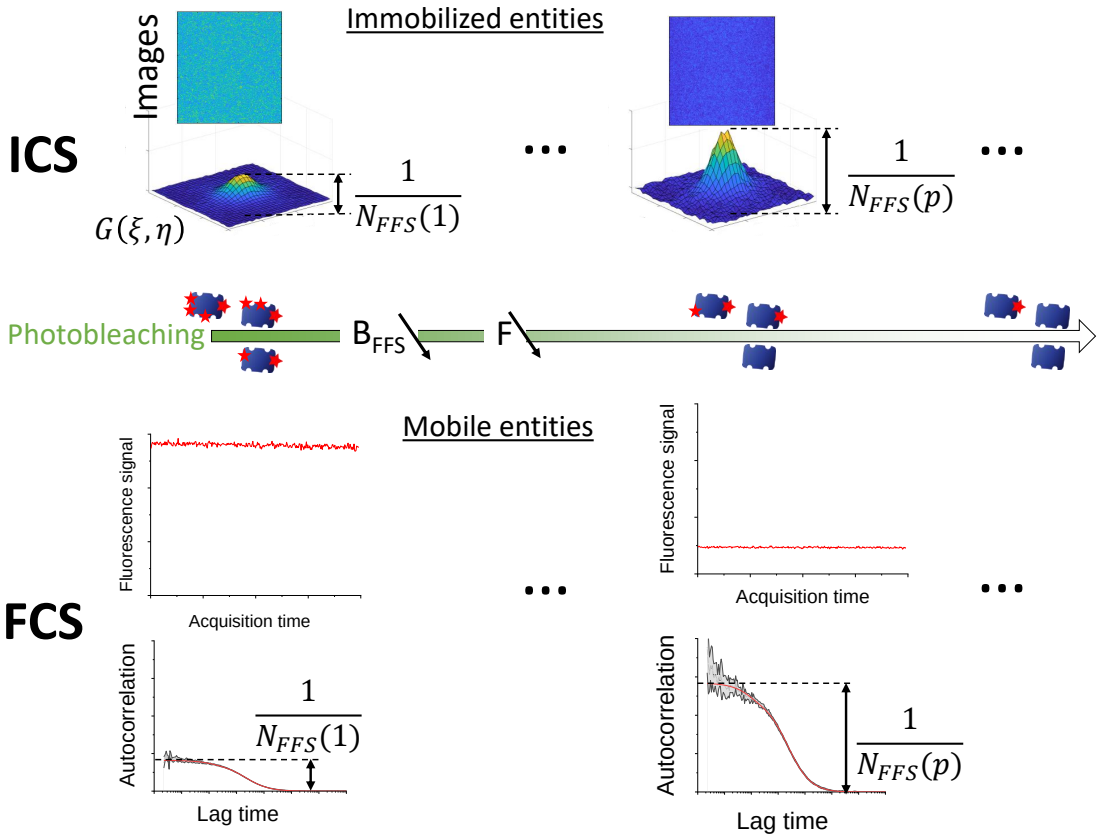

Figure 1: Schematics of the acquisition method, for ICS with immobilized fluorescent entities (top) and FCS with mobile fluorescent entities (bottom): during the photobleaching course, the number of unbleached fluorescent labels (hence the brightness B_{FFS}) decreases, as shown along the graded green central arrow; meanwhile the overall fluorescence signal, F, also decreases, corresponding to the image intensity for ICS or photon count rate for FCS; correspondingly, the number of entities measured by FFS, N_{FFS}, decreases as can be seen by the increased amplitude of the spatial autocorrelation (ICS) or temporal autocorrelation (FCS).

field), are analyzed using the autocorrelation function:

$$G(\xi,\eta) = \frac{\langle \delta F(x,y)\delta F(x+\xi,y+\eta)\rangle}{\langle F(x,y)\rangle^2} \tag{2}$$

In spatial ICS, the fluorescent entities of interest are immobile, so that the autocorrelation is only related to the optical resolution of the microscope (described by the PSF) and is very

well approximated by a Gaussian:[16]

$$G(\xi,\eta) = \frac{1}{N_{FFS}} \exp\left(-\frac{\xi^2+\eta^2}{w_r^2}\right) \tag{3}$$

where N_{FFS} is an apparent mean number of entities in the PSF area of radius w_r. As already pointed out in the introduction (Eq. 1), when the observed species are not equally bright, N_{FFS} is smaller than N, the real number of all the entities. In the case of a mixture of species of different brightness, it can be shown that the FFS techniques leads to:[8,10]

$$N_{FFS} = \frac{(\sum \epsilon_i N_i)^2}{\sum \epsilon_i^2 N_i} \tag{4}$$

where ϵ_i is the brightness of the species i (that is the fluorescence signal of a single entity of the species i) and N_i, the average number of entities of the species i. Note that the true total number of entities is given by $N = \sum N_i$. The key point is that the contributions are weighted by the square of the brightness, leading to an underestimation of the total number of fluorescent entities, when all entities are not equally bright (it's the tree that hides the forest).

Here, we consider that each entity carries several identical fluorescent labels (also named fluorophores). In the forthcoming derivation we shall assume that fluorescence quenching can be neglected, so that the brightness of a single label is constant whatever their number in the entities. In this case, the brightness of an entity carrying n labels is $\epsilon_n = n\epsilon$ where ϵ is the brightness of a single label, and the fluorescence signal reads (N_n being the number of entities that bear exactly n labels):

$$F = \sum n\epsilon N_n \tag{5}$$

The overall brightness, defined as $B_{FFS} = F/N_{FFS}$, is thus given by:

$$B_{FFS} = \epsilon \frac{\sum n^2 N_n}{\sum n N_n} \tag{6}$$

To describe the photobleaching effect, we present a derivation based on the same hypothesis as in the work by Ciccotosto *et al.*[12] We generalize the formalism in order to provide a simple theoretical expression of the brightness for any initial distribution of labels. At a given point during photobleaching, we assume that any fluorophore has the same probability not to be bleached, given by p. This implies that the initial number of labels, n, which appears in Eq. 5 and 6 has to be replaced by the mean number of unbleached labels, which is simply given by np. Therefore the remaining fluorescence signal reads:

$$F(p) = \epsilon \sum npN_n = \epsilon pmN \tag{7}$$

where $m = \frac{1}{N}\sum nN_n$ is the average initial number of labels per entity, computed over all fluorescent entities (this can be called *degree of labelling*). Note that p is nothing but the fluorescence signal normalized to its initial value, before photobleaching has started, i.e. $p = F(p)/F(1)$. In order to also modify Eq. 6 and make it valid all along photobleaching, we need to replace n^2 by its mean value at the fluorescence stage p. Since any fluorescent label can only be in two states, bleached or unbleached, this mean value results from a binomial distribution and equates $np(1-p) + n^2p^2$. As a consequence, Eq. 6 becomes:

$$B_{FFS}(p) = \epsilon \frac{\sum [np(1-p) + n^2p^2] N_n}{pmN} \tag{8}$$

We see that the numerator of Eq. 8 reveals, in addition to the mean value, m, of the initial number of labels per entity, the mean value of its square, $\frac{1}{N}\sum n^2 N_n$ that can be written $\sigma^2 + m^2$, where σ is the standard deviation of the initial number of fluorescent labels

per entity. Consequently, after a few simplifications, Eq. 8 can be written again:

$$B_{FFS}(p) = \epsilon(1 + S_{\sigma m}p) \tag{9}$$

where

$$S_{\sigma m} = \sigma^2/m + m - 1 \tag{10}$$

Hence the measured brightness B_{FFS} is an affine function of the photobleaching stage p: the single label brightness ϵ is its intercept at $p = 0$ (note that this is an immediate output of pbFFS, obtained without any assumption) and $S_{\sigma m}$ is its slope normalized by the single label brightness. Let us rewrite here the equation stating the initial fluorescence signal:

$$F(1) = \epsilon m N \tag{11}$$

Eq. 9, 10 and 11 are the core relations around which all our reasoning is based. Note that studying the variation of the number of entities, instead of the brightness, *versus* the fluorescence signal, would be completely equivalent, as B_{FFS} and N_{FFS} are related through $F = B_{FFS}N_{FFS}$ (we drop out the $_{FFS}$ subscript in F because the fluorescence signal is not biased by fluctuation measurements). We will mostly discuss the brightness because, in absence of background, it always decays as a straight line when plotted as a function of the fluorescence signal (whatever the initial distribution of labels), which is quite convenient for visual inspection of the experimental results. At this stage, it is interesting to make a few remarks about the pbFFS approach.

- First, we emphasize the fact that the parameters σ and m appearing in Eq. 10 and 11 characterize the *initial* distribution of brightness. Of course this distribution varies during photobleaching (it can be shown that it always converges towards a Poisson one), but the slope, $S_{\sigma m}$, depends only on the initial distribution.

- Although $B_{FFS}(p)$ is an affine function of p whatever the initial brightness distribution,

a very peculiar situation is that of entities bearing either no fluorescent label, or exactly one. This leads to $\sigma^2 = m(1-m)$, hence $S_{\sigma m} = 0$ and the measured brightness, $B_{FFS}(p)$, is constantly equal to ϵ, independently of the photobleaching stage. Indeed, all visible entities can only have the brightness of single labels.

- Another notable case is an ensemble of entities that initially bear the same number of labels, say m (this is a single-valued distribution, with $\sigma = 0$). This would lead to a measured brightness, $B_{FFS}(p)$, that linearly varies from $m\epsilon$ to ϵ.

- In all cases, when the fluorescence signal vanishes ($p \to 0$), the measured brightness tends towards the one of a single label ($B_{FFS}(0) \to \epsilon$), since the only entities that remain visible are those bearing one single label. Consequently, one also obtains the total number of fluorophores that is just given by $mN = F(1)/\epsilon$.

- Finally, it is worth to notice that in case of an unknown proportion of dark entities, there is obviously no way to assess it, and thus, to quantify the true total number of entities.

Let us consider now what can be deduced from an experimental photobleaching decay: it yields a measurement of the normalized slope, $S_{\sigma m} = \sigma^2/m+m-1$. This latter value contains all the available information on the initial distribution of labels from a pbFFS experiment. The range of m and σ values compatible with a given measured slope can be represented, in the (σ, m) space, by a half circle of center $(0, \frac{1+S_{\sigma m}}{2})$ and radius $\frac{1+S_{\sigma m}}{2}$, as shown on Fig. 2.

The case of single-valued distributions (all entities bear the same number of labels) corresponds to points along the $\sigma = 0$ vertical axis. Another particular case is that of a Poisson distribution where the mean and the variance are related by $m = \sigma^2$, as depicted in Fig. 2. In this case, the photobleaching decay provides all necessary information to define the distribution. The measured brightness becomes $B_{FFS}(p) = \epsilon(1 + mp)$, which is the same expression as the one obtained in Ref.,[11] but it is derived here in a more general framework. Note that,

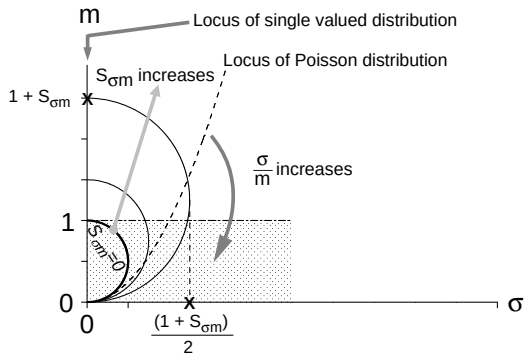

Figure 2: Geometrical representation of the relation between the mean, m, and the standard deviation, σ, of the *initial* number of labels per entity; for a given measured slope, $S_{\sigma m}$, the (σ, m) points are distributed along a half circle of diameter $1 + S_{\sigma m}$, which always crosses the $(0, 0)$ point; the ratio $\frac{\sigma}{m}$ continuously increases from the top to the base of the half-circle. The particular case of a single-valued distribution corresponds to points located on the vertical axis ($\sigma = 0$); the smallest circle, of diameter 1, corresponds to entities bearing either no fluorescent label, or a single one ($S_{\sigma m} = 0$); in the case of a Poisson distribution, the solution is at the intersection of the corresponding dashed line ($m = \sigma^2$) and the half circle of diameter $1 + m$ (see text). If all molecules are labelled, there are no (σ, m) solutions in the lower half space, below the dashed-dotted line $m = 1$.

for small degrees of labelling, the percentage of unlabelled species can be very large since, according to the properties of the Poisson distribution, it is given by e^{-m}.

In the general case where $S_{\sigma m} > 0$, the photobleaching slope can only provide a lower limit of the true number of entities N (and hence the surface density) but no upper bound: since $N = F(1)/m\epsilon$, the condition $m \leq 1 + S_{\sigma m}$ (see Fig. 2) leads to a lower bound, which equals the apparent value $N_{FFS}(1) = F(1)/B_{FFS}(1)$ (corresponding to the case where all entities have the brightness $B_{FFS}(1) = (1 + S_{\sigma m})\epsilon$). The fact that the real N cannot be lower than the apparent N_{FFS} is not new, since we argued that a distribution of brightness *always* causes FFS to underestimate the number of entities (Eq. 1). An upper bound for N can be established if we consider only *fluorescent* entities: in this case, the minimum value of m is larger than 1. Therefore, the true number of *fluorescent* entities is included between $N_{FFS}(1)$ and $F(1)/\epsilon = (1 + S_{\sigma m})N_{FFS}(1)$.

To summarize, the pbFFS method is useful if the initial label distribution can be fully

described by a limited number of degrees of freedom. When there is only one, the label distribution can be estimated from the photobleaching slope, which makes it possible to determine the true number of entities. This is for instance the case for a Poisson law, as already used for DNA or fibrinogen labelling.[11,14] Another example is that of a sample where all entities are uniformly labelled. When the number of degrees of freedom of the distribution is two, it may nevertheless be possible to infer a range of values for the number of entities, by combining the constraints of the label distribution with the relation between σ and m as established by the measured slope. This is the case encountered in the current work with SAv molecules, which are assumed to bear 1, 2 or 3 fluorescent labels.

Methods

Substrate preparation

Microscopy glass coverslips (24×24 mm, Menzel Gläser) were cleaned under sonication with acetone and isopropanol and blow-dried with nitrogen. They were UV/ozone activated (UV/Ozone ProCleaner Plus, Bioforce) for 10 min, attached to a microscopy support and PLL(20)-g[3.5]-PEG(2)/PEGbiotin(3.4)50% (≈107 kDa, SuSoS AG) was incubated at 10 μg/ml in 10 mM Hepes buffer (Fisher, pH=7.2) for 45 min.[17] Streptavidin (≈55kDa, Sigma Aldrich), SAv, and streptavidin Alexa Fluor™555 conjugate (≈55kDa, Molecular probes), SAv-Alex, with a labeling degree of 2 (certificate of analysis, Molecular probes) were mixed in a ratio varying from 100:1 to 100:100 at 10 μg/ml in Hepes buffer and incubated for 30 min. A layer of biotinylated species was prepared by immobilizing Atto-labelled biotin (Atto 565-Biotin, 921 Da, Sigma-Aldrich), bAtto, to a saturated layer of SAv, bAtto occupying the free biotin pockets on SAv. In all cases, the sample was rinsed 5 times with Hepes after incubation.

Confocal imaging and photobleaching of surfaces

Functionalized glass coverslips were imaged using a Leica SP8 confocal microscope with a HC PL APO 63×1.2 water-immersed objective. The focal plane was determined where intensity was at maximum and then stabilized using the Adaptive Focus Control mode. The signal was detected with a hybrid detector working in the photon counting mode. An area of 25×25 μm^2 with 512×512 pixels was imaged 10 times with a pixel dwell time of 5 μs and a reduced laser intensity at 561 nm, so not to saturate and not to bleach the sample during image acquisitions. Then, this area was photobleached with a sufficient illumination dose (scanning time×laser power) to loose roughly 30% of the initial signal and 10 images were acquired as before. This procedure was typically repeated 6 to 8 times, in order to finish the acquisition with a remaining signal of at most 10% of the initial one.

ICS analysis

Before performing ICS analysis, it is necessary to correct the non-uniformity of the image intensity in the 1 - 10 μm scale range because, as already discussed in,[14] it can have a strong impact on the autocorrelation function. This non-uniformity originates, either from a spatial dependence of the light efficiency of the imaging system, or from an inhomogeneous surface density. It induces long range correlations that add to the autocorrelation of interest with various detrimental effects, such as anomalous base line, width and long range behaviour. Image flattening is especially crucial when the surface density is very high and thus the autocorrelation very weak, because in this case the relative bias can be very pronounced. In order to leave the ratio of the fluctuation amplitude to the mean value unchanged, on which the estimated number of entities depends, the images are flattened by dividing them by their own smoothed version. The latter is obtained by convoluting the original image with a two-dimensional Gaussian function. The width of this Gaussian has to be small enough to damp as much as possible image inhomogeneities, but significantly larger than the radius of the ICS PSF area ($w_r \approx 0.23\mu m$), in order not to bias the number fluctuations. Consistently

with our previous study,[14] the $1/e$ half width of the Gaussian function used to smooth and flatten the images was chosen to be 2 μm. In practice, the images are individually flattened and autocorrelated. Then, for each photobleaching stage, the mean autocorrelation is fitted with Eq. 3, which gives a global estimation of N_{FFS} and the radius w_r. By verifying that the latter varies by much less than 1%, we check the stability of the focus during the acquisition process. The final goal being to analyze the variation of the brightness, B_{FFS}, *versus* the fluorescence signal F (i.e. the intensity), the images are divided in 8×8 sub-images that are individually analyzed by ICS, while the value of the radius w_r is set at the one estimated from the whole image, thus providing a mean and a standard deviation of the mean of the brightness at each photobleaching stage. The image processing (flattening, autocorrelation and fit) was performed using Matlab (Mathworks).

Sample preparation for photobleaching of solutions

To achieve photobleaching of the fluorophores in solution in a reasonable amount of time (a few minutes), with the available laser power ($\leq$1 mW), the solutions were confined in poly(dimethylsiloxane) (PDMS) microwells. A regular array containing pillars of 100 μm in diameter and 100 μm in height with a pitch of 400 μm was fabricated on the Si wafer. After peeling off the mold, the 2 mm thick PDMS micropatterned slabs were activated with air plasma (Atto, Diener) for 2 min to achieve a hydrophilic surface.[11] Then a droplet of SAv-Alex or bAtto Hepes solution was placed on the PDMS block to enter the microwells, at initial concentrations around a few 100 nM. Such concentrations, relatively high for FCS, were necessary to saturate the microwell walls and avoid too much adsorption/desorption processes that induce unstable fluorescence signal. For control purposes, we also used solutions of Sulforhodamine B sodium salt, SRB (Sigma-Aldrich, St. Louis, USA), without further purification, diluted in either deionised water or Hepes. The PDMS block was flipped onto a Lab-Tek™Chambered Coverglass (Nunc) to seal the microwells and thus avoiding fluid exchange with the environment.

FCS acquisition and analysis

The signal inside the microwells was acquired using a Nikon confocal microscope (Ti2E - A1R) with a 60×water-immersed objective and a reduced laser power at 561 nm, to avoid any photobleaching during FCS acquisitions. The latter were performed using a custom made detection system, comprising a 50/50 beam splitter and a pair of avalanche photodiodes (SPCM-AQRH-44-FC, EXCELITAS) to avoid after-pulsing effects, which was connected on the auxiliary port of the microscope using a multimode optical fiber. The focal plane was set at 20 μm inside the microwells and photons were counted during 5 periods of 20 s to provide an averaged cross-correlation curve (and its corresponding standard error of the mean) using a Correlator.com software (Flex99r-12D). Proper optical adjustments and stability were controlled by fitting the diffusion time[18] and measuring the brightness of a reference dye, namely sulfo-rhodamine B. Each FCS acquisition thus gives an estimation of the number of entities, N_{FFS} and of the corresponding brightness, B_{FFS}, with a given uncertainty; it was followed by a bleaching cycle with a laser intensity adjusted to typically reduce the initial signal by 30% before performing the next acquisition. This was repeated 5 to 8 times until about less than 10% of the initial signal remains, in order to provide the variation of the brightness, B_{FFS}, with error bars, *versus* the fluorescence signal F (or photon count rate).

Summary of acquisition and analysis methods

As described above and summarized in Fig. 3(A), from the series of ICS or FCS analysis at various photobleaching stages, one obtains the variation of the brightness versus the fluorescence signal. Sometimes, we observed, both on surface and in solution, photobleaching decays that do not exhibit a linear behavior (as the red line), but drop down to lower values of the brightness when the fluorescence signal gets small (green curve). This is due to an uncorrelated background, BG, that contributes to the detected signal, thus making the relative fluctuations smaller and consequently the apparent number of entities larger, hence a lower brightness. It is nevertheless possible to incorporate the background as a free parameter

in the photobleaching decay analysis by rewriting Eq. 9 as:

$$B_{FFS}(p) = \epsilon \left(1 - \frac{r_{BG}}{p}\right) \left(1 + S_{\sigma m} \frac{p - r_{BG}}{1 - r_{BG}}\right) \tag{12}$$

where $r_{BG} = BG/F(1)$ stands for the background normalized to the total initial signal (i.e. including the background itself). Correspondingly, p becomes the relative total signal, including the background. The latter originates, either from light scattering (due to the glass substrate or to the walls of the PDMS microwells), or from some bulk fluorescence that would be not properly filtered out by the confocal detection. This effect appeared to be especially pronounced and difficult to mitigate in solutions.

As a result, the fit of the photobleaching decay shown in Fig. 3(A) gives the parameters ϵ, $S_{\sigma m}$ (and BG, if relevant). The degree of labelling of SAv-Alex given by the manufacturer being 2, we take this number as an approximate value and consider that each SAv protein can bear 1, 2 or 3 Alexa labels. The key point is that this distribution has only 2 independent degrees of freedom (since, once the probabilities of 1 and 2 labels are known, the probability of 3 labels automatically follows). As a consequence, since m and σ are not independent but linked through Eq. 10, the range of possible m and σ values is limited. In our current situation, it can be shown (see Supporting Information, Section S1, Eq. S1 to S5 and Fig. S1) that if $S_{\sigma m} \leq 1$, then $\frac{3}{3-S_{\sigma m}} \leq m \leq \frac{2}{2-S_{\sigma m}}$, while if $1 < S_{\sigma m} \leq 2$, then $\frac{3}{3-S_{\sigma m}} \leq m \leq \frac{6}{4-S_{\sigma m}}$ (we never measured $S_{\sigma m} > 2$). Fig. 3(B) schematically shows a few examples of distributions, which correspond to the value $S_{\sigma m} = 0.8$ that is often found, spanning from the narrowest distribution (minimum value of σ), with the largest mean value, m, to the widest one, with the smallest m. Interestingly, if we were hypothesising that SAv proteins could bear 2, 3 or 4 Alexa labels, this would lead to, either no solution when $S_{\sigma m} < 1$ and, for the few cases where we measured $1 \leq S_{\sigma m} \leq 1.5$, to a large majority of SAv molecules bearing 2 Alexa labels and almost none bearing 3 or 4, which is consistent with the model retained throughout this work (see Section S1 of Supporting Information, Eq. S6). Concerning the

biotinylated fluorescent molecules, it is clear from the bAtto formula (given in the product specification) that they correspond to one single Atto dye. However, as already noted above, as a SAv protein of the base layer exposes from 1 to 3 free biotin binding sites, several bAtto molecules can colocalize on a single SAv protein. Therefore, we also assume that biotinylated entities can bear 1, 2 and 3 fluorophores. To conclude, from the analysis of the brightness decay, we obtain a range of values for m, and hence a range of values for the true number of fluorescent entities, $N = F(1)/m\epsilon$, which in turn leads to the final surface density given by $N/\pi {w_r}^2$.

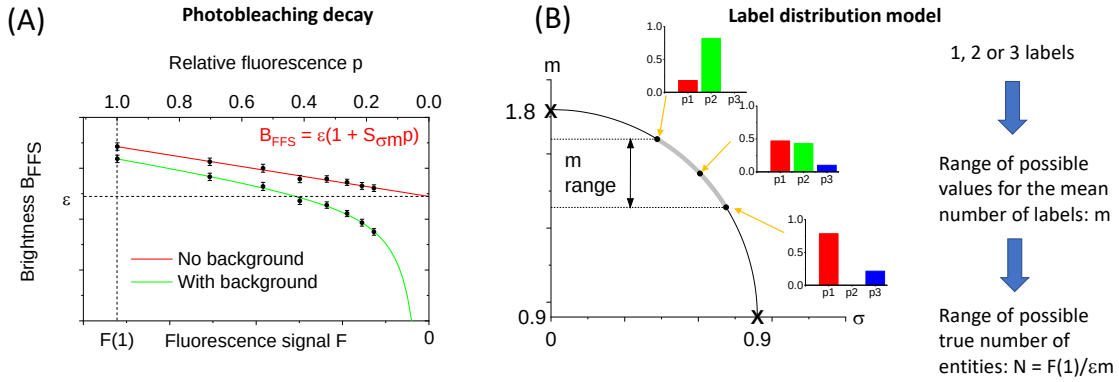

Figure 3: Principle of the brightness decay analysis: (A) Upon photobleaching, the brightness, B_{FFS}, decreases linearly *versus* the fluorescence signal, F or p (red solid line), except in the presence of a background, which can be taken into account in the fit (green solid line) that provides the output parameters ϵ and $S_{\sigma m}$. (B) By combining the relation between m and σ corresponding to $S_{\sigma m}$ and the constraints induced by a distribution over 1, 2 or 3 labels, the possible m values are contained in a limited range; 3 examples of distributions corresponding to the minimum, maximum and central values of m are depicted for $S_{\sigma m} = 0.8$; it is noteworthy that a distribution like the one obtained for the minimum value of m, where no entities bears 2 labels, is obviously unrealistic, while the 2 other distributions are acceptable. Finally, this analysis provides a value of the mean number of labels, m which, combined with the initial fluorescence signal, $F(1)$ and the parameter ϵ, leads to an estimation of the true number of entities, N.

Experimental results

Measurements on streptavidin

Streptavidin layers are densely packed

Photobleaching ICS experiments have been performed on SAv layers with controlled percentages of labelled SAv (SAv-Alex) of 1%, 10%, 50% and 100%. Since ICS usually performs better for relatively low surface densities, these dilutions aimed at testing the robustness of our method in a range of densities relevant for biomimetic surfaces.

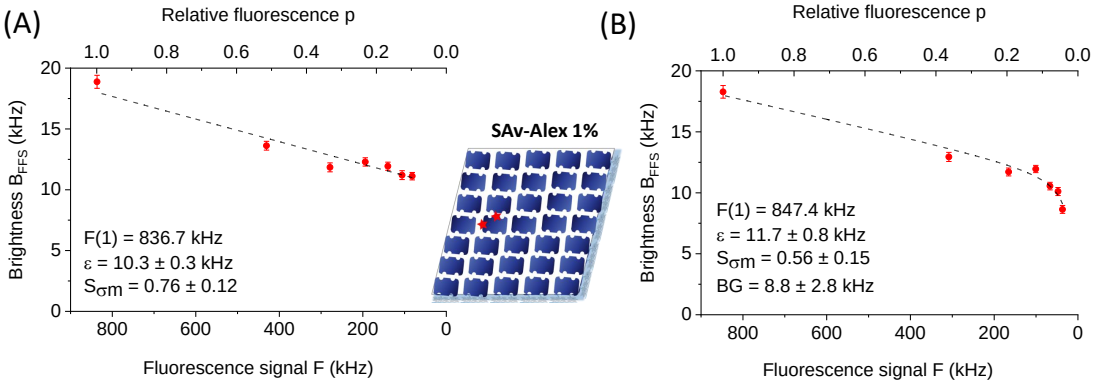

Figure 4: Characteristic brightness decay *versus* the fluorescence signal for a SAv layer prepared with a 1% dilution of SAv-Alex. (A) Example without background, showing the linear decay and the fit (dashed black line) with the ϵ and $S_{\sigma m}$ outputs corresponding to the measured (red) points; the errors bars are the standard errors of the mean calculated from the 8×8 sub-images; (B) In presence of background, the corresponding parameter, BG, can be fitted (it represents about 1% the initial fluorescence signal, $F(1)$), while the other outputs, ϵ and $S_{\sigma m}$, are consistent with the results of the background-free case.

We see in Fig. 4(A) a plot of a characteristic brightness decay *versus* the fluorescence signal obtained for 1% dilution of SAv-Alex. The parameters estimated from the fit, $\epsilon = 10.3$ kHz and $S_{\sigma m} = 0.76$, correspond to an initial brightness, given by $B_{FFS}(1) = \epsilon(1+S_{\sigma m})$, that is about 1.8 times larger than the single label brightness. Consequently, if the distribution of the number of labels per molecule was single-valued, one would be close to the situation of 2 Alexa dyes per SAv, which corresponds to the manufacturer specifications. However, using the theory presented above, we can estimate the range of m values (compatible with both the

possible numbers of labels and the estimated value of $S_{\sigma m}$) at $[1.34, 1.61]$ (see Supporting Information, Fig. S1 and Eq. S4). We can even push further our reasoning by visually inspecting, in Fig. 3(B), the distributions of labels obtained for $S_{\sigma m}$ values slightly smaller than 1. Clearly, a distribution close to that of the limiting case with the smallest mean value, m, and largest width, σ, is unrealistic, as it would correspond to SAv proteins that never bear 2 labels, while most of them bear 1 label and some 3! It can be shown (Supporting Information, Section S1) that the condition for SAv to have a smaller probability to bear 3 labels than 2, implies $m > \frac{1}{1-\frac{3}{8}S_{\sigma m}}$. With this additional constraint, the m range is further restricted to $[1.40, 1.61]$, which leads to a surface density of labelled SAv, at 1% dilution, in the range of 316-363 molecules per μm^2 (using w_r= 0.22 μm for this data set). We also show, in Fig. 4(B), another result obtained with the same dilution of SAv-Alex, but exemplifying the consequence of a background on the brightness decay. Although the background accounts only for about 1% of the total initial signal, the deformation from linearity of the brightness decay is very pronounced at the end of the process. However, the decay can still be well fitted using one additional parameter, BG, while the other parameters remain consistent with their values estimated without background.

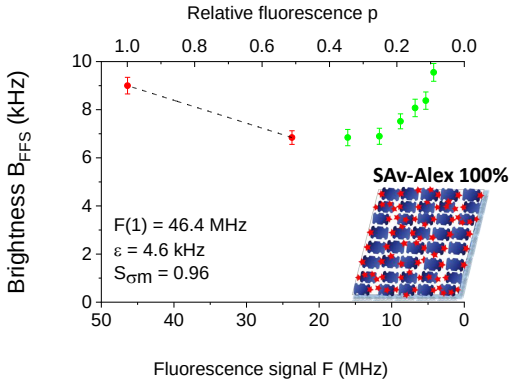

Figure 5: Example of the dramatic consequence, for the brightness decay, of the fluorescence quenching between Alexa555 fluorophores of a streptavidin layer prepared with 100% of SAv-Alex. Note that the single label brightness, ϵ, is more than twice smaller than its value at high dilution (see Fig. 4), while the $S_{\sigma m}$ parameter, estimated from the 2 first points, stays consistent.

A physically different situation occurs at high surface densities of labelled SAv, as shown in Fig. 5 for a layer containing 100% of SAv-Alex. This curve exhibits a dramatic brightness recovery after an initial decay. By fitting the first part of the brightness variation, assumed to be linear, we estimated the $S_{\sigma m}$ parameter at a value, 0.96, reasonably close to the one measured at 1% dilution. Conversely, the single label brightness, $\epsilon = 4.6$ kHz, is found to be more than 2 times lower than the value measured at high dilutions of SAv-Alex (see Fig. 4). We suggest that fluorescence quenching between identical fluorophores can explain this behavior: at 100% concentration, the mean distance between the Alexa555 dyes is of the order of the size of the streptavidin molecules, that is ≈ 5 nm. At such short distances, the reduction of the fluorescence quantum yield can be very pronounced.[19] When photobleaching occurs, the mean distance between intact fluorophores increases, thereby reducing self-quenching so that the brightness tends towards its normal value. Because this is not within the scope of the present work, we did not study further the exact shape of the brightness curve, but we tentatively made use of the 100% concentration results to estimate the surface density of SAv. Using the waist size found for this 100% SAv-Alex case, $w_r = 0.25\mu m$ and $m = 1.7$ (middle of the range corresponding to $S_{\sigma m} = 0.96$), we estimate 30330 streptavidin molecules per μm^2. First, this number is close to 100 times the surface density measured at 1% dilution. Second, it corresponds to a mean distance of 5.7 nm between streptavidins, which is consistent with the assumption of a densely packed layer, given the size of a streptavidin molecule.[20] Therefore, although based solely on the first 2 points, the results obtained for 100% of labelled SAv are compatible with the lower-density case. Experiments have also been performed with 10% and 50% dilutions, the results of which are reported and synthesized in Table 1. Overall, our SAv-Alex results are consistent with each other, with a clear trend towards more fluorescent quenching as the surface density of SAv-Alex increases.

Streptavidin in solution has the same label distribution

As the principle of pbFFS is not specific to molecules immobilized on surfaces, we also applied our method to SAv-Alex molecules freely diffusing in solution, to get an independent estimation of the parameter $S_{\sigma m}$. We found a value of $S_{\sigma m}$ very consistent with the estimations on surfaces (around 0.8), as illustrated in Fig. 6(A). As a control case, Fig. 6(B) shows that SRB solutions lead to a constant brightness when photobleaching, as expected for a single dye molecule.

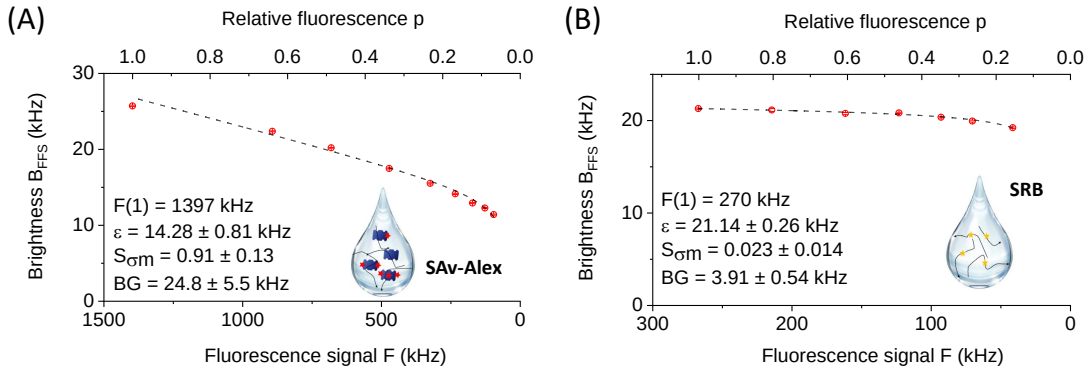

Figure 6: Examples of brightness decays measured by FCS, for solutions confined in PDMS microwells. (A) SAv-Alex molecules, where the relative slope, $S_{\sigma m}$, is close to its value found on surfaces (see Fig. 4); (B) SRB in HEPES, clearly showing an almost constant brightness, in agreement with the expected behavior of a single dye molecule. For both cases a background of up to 2% is estimated. Note that the error bars are smaller than the point size.

Measurements on biotinylated molecules

Biotinylated molecules bind to about 10% of the streptavidin base layer

Next we investigated the surface density of biotinylated molecules deposited on top of SAv layers, in order to show the potential of pbFFS as a characterization tool for developing biomimetic surfaces. Fluorescent bAtto molecules bound on a streptavidin base layer were observed. The brightness decay, as shown in Fig. 7(A), exhibits a normalized slope, $S_{\sigma m} = 0.21$, which is significantly smaller than the one observed for a SAv-Alex layer. This means

that this case is close to the one of a single fluorophore per labelled SAv. Assuming the same type of distribution (i.e. over 1, 2 or 3 labels), the range of m values that corresponds to $S_{\sigma m} = 0.21$ is estimated to $[1.08, 1.12]$ (see Supporting Information, Fig. S1 and Eq. S4). Two quantities can be estimated from these measurements: the surface density of bAtto molecules (given by $F(1)/\epsilon\pi {w_r}^2$), which is 3708 molecules per μm^2, and the density of *labelled* SAv (given by $F(1)/(m\epsilon\pi {w_r}^2)$ with $m = 1.1$, center of the range estimated above), which is approximately $3370/\mu m^2$. Since we found previously ∼30330 SAv per μm^2 in the base layer, this implies that about 1 in 10 SAv molecules can carry a bAtto molecule.

Each SAv has 4 biotin binding sites: at least one of these is used to bind to the PLL-g-PEGbiotin base layer, so that the *a priori* number of available sites for bAtto is between 0 and 3. Our data indicate that many SAv molecules could not bind any bAtto, presumably due to steric hindrance. Among the *labelled* SAv, a large majority bound only one bAtto, but a few bound more than one (since the average number of bAtto per fluorescent SAv is ∼1.1): at least 88% of fluorescent SAv bear a unique bAtto and at most 12% have two. Two mechanisms can lead to this distribution: either bAtto bind to SAv as single molecules, in which case a few SAv have more than one occupied biotin-binding pocket, or bAtto preexist as dimers, trimers, etc. in the solution used for incubation, in which case, SAv may present only one pocket occupied by a bAtto complex. Indeed, the fact that Atto dyes are moderately hydrophilic[21] could favor aggregation.

To assess bAtto aggregation in solution, we performed pbFFS experiments with bAtto solutions (FCS), as reported in the next paragraph.

Biotinylated molecules slightly aggregate in solution

When performing photobleaching experiments with bAtto in solution, we recovered values close to those found on surface (i.e. $S_{\sigma m} \approx 0.2 - 0.3$), as can be seen in Fig. 7(B) and summarized in Table 1, which is clearly distinct from the single molecule case of SRB in solution shown in Fig. 6(B). The above range of values for $S_{\sigma m}$ corresponds to a mean number

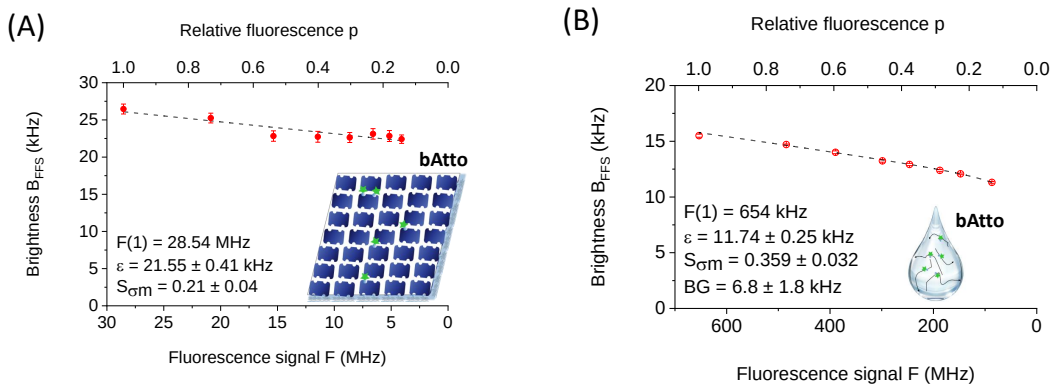

Figure 7: Brightness decay of biotinylated fluorescent molecules (bAtto), measured on surface and in solution. (A) ICS measurements for bAtto bound to a streptavidin base layer, exemplifying the lower relative slope value, $S_{\sigma m} = 0.21$, compared to SAv-Alex (The fact that bAtto exhibits a single label brightness different from that of Alexa555 labelled SAv is only due to the photophysical properties of these dyes); (B) FCS measurements for bAtto freely diffusing in solution, giving a slope close to that on surface. Note that the error bars are smaller than the point size.

of labels per diffusing entity, m, between 1 and 1.2 (see Supporting Information, Fig. S1). Since one bAtto molecule definitively corresponds to a single Atto dye, we conclude that unspecific aggregation occurs between bAtto molecules in solution, despite the moderate concentration ($< \mu$M). As a consequence, although the concentrations used to incubate the SAv base layer with bAtto are much lower than those used for FCS experiments (which should mitigate the aggregation trend), we cannot exclude that each SAv has only one bAtto binding site occupied by an aggregate. In this case, the number of available biotin binding sites on the SAv layer is not that of the number of bound bAtto molecules (i.e. 3708 / μm^2) but rather that of the number of SAv molecules labelled with bAtto (i.e. 3370 / μm^2).

Note that the difference in brightness between bAtto in solution and on a SAv layer, shown in Fig. 7, is not relevant, as the ICS and FCS experiments are performed on surface and in bulk, respectively (with different microscopy setup). The same remark stands for SAv results shown in Fig. 6(A) and Fig. 4.

Table 1: Degree of labelling (m values) and areal mass density (when applicable) measured for different molecules, on surface and in solution, with pbFFS and ellipsometry.[22] For diluted SAv-Alex molecules, the estimated areal mass density is linearly extrapolated to 100% SAv. Values are given as mean ± SD

			Density (ng^2/cm^2)	
Molecule	**Sample**	**Labelling**	**pbFFS**	**Ellipsometry**
SAv-Alex	Surface 100%	1.79 ± 0.39	239 ± 34	253 ± 33
SAv-Alex	Surface 50%	1.22 ± 0.05	303 ± 50	n/a
SAv-Alex	Surface 10%	1.94 ± 0.22	293 ± 69	n/a
SAv-Alex	Surface 1%	1.78 ± 0.38	323 ± 28	n/a
SAv-Alex	Solution	1.58 ± 0.18	n/a	n/a
bAtto	Surface	1.13 ± 0.09	0.82 ± 0.23	n/a
bAtto	Solution	1.125 ± 0.057	n/a	n/a
SRB	Solution	1.013 ± 0.011	n/a	n/a

pbFFS results agree with ellipsometry

We present in Table 1 the degree of labelling (m) corresponding to the data obtained in various conditions (SAv-Alex, bAtto and SRB molecules, in solution and on surfaces). For each condition, all the m values where pooled to give a mean and a standard deviation. When applicable, these values were then used to derive the areal mass density of SAv molecules. The pbFFS estimation of the density of 100% SAv-Alex is in fairly good agreement with spectroscopic ellipsometry results[22] (QCM-D data are not reported as they would correspond to an hydrated mass[3]). Concerning bAtto, the areal mass density corresponds to the total number of bAtto bound to SAv molecules, which is independent of the m value of SAv molecules that are labelled with bAtto.

Discussion

We have presented a method, named pbFFS, which aims as estimating the number density of entities of non uniform brightness. We have shown its potential for more reliable quantification of surface density in the context of biomimetic layer characterization. Hereafter, we discuss two limiting situations.

In this work, we have measured surface densities spanning two orders of magnitude, from ∼300 to ∼30000 molecules per μm^2. This latter value is probably close to the highest density that can be measured using ICS. Indeed, at high concentration/density of molecules, the relative intensity fluctuations and thus, the autocorrelation amplitude, are very small and may be hidden behind unwanted variations (non-uniformity of the imaging system or the sample). Therefore, it is quite important to properly flatten images, check stability of solutions, etc. High densities can also induce some detrimental photophysical effects, such as quenching. However, we experimentally showed that this does not prevent correct results, provided the biased data points are taken off from the analysis.

The streptavidin molecules studied here were labelled by 1 to 3 fluorophores, so the degree of labelling was rather low. One may wonder whether pbFFS would also be suitable for studying entities with a higher degree of labelling (several tens of fluorophores or more). In this case, the photobleaching process starts with entities that are initially very bright and must be carried out till only single labels are left, which requires a high dynamic range of detection. Using fluorescent microspheres we could check that, in principle, our framework also applies in such situations, as shown in Supporting Information, Section S2.

Besides number density quantification, some applications may benefit from the ability of pbFFS to provide information on the degree of labelling (or number of fluorophores per entity). This would be the case of oligomerization studies. Oligomerization is an ubiquitous phenomenon that plays an important role in numerous biological processes. The size of oligomers is usually estimated using fluorescence fluctuation methods (FCS, ICS) by comparing the measured brightness to the one found on a sample containing only monomers, in the same experimental conditions. Such a method suffers from two drawbacks: first, a reference sample with only monomers may not be easily available; second, if all the oligomers do not have the same size, the result is biased resulting in an overestimation of the oligomer size. The pbFFS method does not require a separate measurement on monomers, since the monomer brightness (ϵ) is provided by the fit: it is *self-calibrated*, which is a significant

advantage. Moreover, some information on the distribution of oligomer size can be obtained, although, as shown in this work, the exact distribution can only be resolved if the number of degrees of freedom is reduced by additional assumptions (*e.g.* only few possible oligomers). This strategy would work not only on fixed samples, but also in living cells. As a matter of fact, it has been recently proposed to make benefit of photobleaching in live cell to retrieve molecular brightness and to turn confocal images into concentration maps.[23] However this method cannot be used in cases when the studied protein forms homo-oligomers, contrarily to the present work.

Finally, we point out that, while our method contrasts with standard semi-quantitative fluorescence approaches that cannot deal with a distribution of brightness, it can be compared with some single molecules techniques based on stepwise photobleaching.[5] For instance, Madl et al. performed a combination of photobleaching and brightness analysis to measure the subunit composition of membrane proteins.[24] However, single molecules techniques obviously require extremely low surface density of immobilized molecules, while pbFFS works in the much higher density regimes, which is more relevant for most biomimetic and biological samples. Nevertheless, in a recent work, Stein et al. have combined FCS with single-molecule localization microscopy, to provide the quantification of target molecules independent of the localization cluster density.[25]

Conclusion

In this paper we presented a method, combining fluctuations analysis and photobleaching, that aims at characterizing molecules or particles labelled with a unknown distribution of fluorophores. pbFFS can be used both on surfaces or in volume, with immobilized or moving molecules (either in flow or freely diffusing). It provides the single label brightness, as well as a parameter depending on the mean and variance of the distribution of labels. If additional assumptions can be used to restrict the number of degrees of freedom of this distribution,

the degree of labelling and an unbiased value of the concentration or density can be deduced.

The pbFFS method has been demonstrated on a SAv base layer of biomimetic samples to estimate the surface density of SAv, and its propensity to bind a top layer of bAtto molecules. For the base layer density, the density estimated with pbFFS is in agreement with ellipsometry measurements. However, compared to this latter technique or QCM-D, pbFFS has the advantage of allowing *in situ* characterization, since it does not require dedicated substrates, and the quantification of low mass of adsorbed molecules (as in the case of bAtto), out of reach of the other techniques, thanks to the intrinsic sensitivity of fluorescence measurements.

We believe pbFFS can provide a powerful framework to attain more reliable fluorescence fluctuations analysis: indeed, standard FFS techniques are completely unable to assess whether their results are biased by a dispersion of brightness values (or number of labels), whereas, using pbFFS, the linear decay of the brightness during photobleaching is a simple checkpoint, which contributes to making the measurements more trustworthy.

In addition to number density estimations, the capability of pbFFS to evaluate the number of fluorophores per entity should make it particularly useful for oligomerization studies, with the aim to determine the oligomers sizes.

Acknowledgement

We acknowledge D. Centanni (LIPhy) for the microwell preparation and the IAB facility for the confocal microscope. We thank M. Balland (LIPhy) and O. Destaing, A. Grichine (IAB) for stimulating discussions. We acknowledge E. Castro Ramirez for her work with PLL-g-PEGb. The project is funded by ANR GlyCON ANR-19-CE13-0031-01.

Supporting Information Available

Theoretical derivation of occupancy probabilities; Results of experiments with 20 nm fluorescent beads and corresponding analysis (PDF).

References

(1) Martino, M. M.; Briquez, P. S.; Maruyama, K.; Hubbell, J. A. Extracellular matrix-inspired growth factor delivery systems for bone regeneration. *Advanced Drug Delivery Reviews* **2015**, *94*, 41–52.

(2) Migliorini, E.; Guevara-Garcia, A.; Albiges-Rizo, C.; Picart, C. Learning from BMPs and their biophysical extracellular matrix microenvironment for biomaterial design. *Bone* **2020**, *141*, 115540.

(3) Sefkow-Werner, J.; Machillot, P.; Sales, A.; Castro-Ramirez, E.; Degardin, M.; Boturyn, D.; Cavalcanti-Adam, E. A.; Albiges-Rizo, C.; Picart, C.; Migliorini, E. Heparan sulfate co-immobilized with cRGD ligands and BMP2 on biomimetic platforms promotes BMP2-mediated osteogenic differentiation. *Acta Biomaterialia* **2020**, *114*, 90–103.

(4) Waters, J. C.; Wittmann, T. *Methods in Cell Biology*; Elsevier, 2014; pp 1–18.

(5) Verdaasdonk, J. S.; Lawrimore, J.; Bloom, K. *Methods in Cell Biology*; Elsevier, 2014; pp 347–365.

(6) Slaughter, B. D.; Li, R. Toward Quantitative "In Vivo Biochemistry" with Fluorescence Fluctuation Spectroscopy. *Molecular Biology of the Cell* **2010**, *21*, 4306–4311.

(7) Hennen, J.; Saunders, C. A.; Mueller, J. D.; Luxton, G. W. G. Fluorescence fluctuation spectroscopy reveals differential SUN protein oligomerization in living cells. *Molecular Biology of the Cell* **2018**, *29*, 1003–1011.

(8) Kolin, D. L.; Wiseman, P. W. Advances in Image Correlation Spectroscopy: Measuring Number Densities, Aggregation States, and Dynamics of Fluorescently labeled Macromolecules in Cells. *Cell Biochemistry and Biophysics* **2007**, *49*, 141–164.

(9) Kitamura, A.; Kinjo, M. State of the Art Fluorescence Fluctuation Based Spectroscopic Techniques for the Study of Protein Aggregation. *International Journal of Molecular Sciences* **2018**, *19*, 964.

(10) Müller, J. D. Cumulant Analysis in Fluorescence Fluctuation Spectroscopy. *Biophysical Journal* **2004**, *86*, 3981–3992.

(11) Delon, A.; Wang, I.; Lambert, E.; Mache, S.; Mache, R.; Derouard, J.; Motto-Ros, V.; Galland, R. Measuring, in Solution, Multiple-Fluorophore Labeling by Combining Fluorescence Correlation Spectroscopy and Photobleaching. *The Journal of Physical Chemistry B* **2010**, *114*, 2988–2996.

(12) Ciccotosto, G. D.; Kozer, N.; Chow, T. T.; Chon, J. W.; Clayton, A. H. Aggregation Distributions on Cells Determined by Photobleaching Image Correlation Spectroscopy. *Biophysical Journal* **2013**, *104*, 1056–1064.

(13) Paviolo, C.; Chon, J. W. M.; Clayton, A. H. A. *Advances in Experimental Medicine and Biology*; Springer Singapore, 2018; pp 41–52.

(14) Mets, R. D.; Wang, I.; Gallagher, J.; Destaing, O.; Balland, M.; Delon, A. Determination of protein concentration on substrates using fluorescence fluctuation microscopy. Single Molecule Spectroscopy and Superresolution Imaging VII. 2014.

(15) Dundas, C. M.; Demonte, D.; Park, S. Streptavidin–biotin technology: improvements and innovations in chemical and biological applications. *Applied Microbiology and Biotechnology* **2013**, *97*, 9343–9353.

(16) Petersen, N.; Höddelius, P.; Wiseman, P.; Seger, O.; Magnusson, K. Quantitation of membrane receptor distributions by image correlation spectroscopy: concept and application. *Biophysical Journal* **1993**, *65*, 1135–1146.

(17) Huang, N.-P.; Vörös, J.; Paul, S. M. D.; Textor, M.; Spencer, N. D. Biotin-Derivatized Poly(l-lysine)-g-poly(ethylene glycol): A Novel Polymeric Interface for Bioaffinity Sensing. *Langmuir* **2002**, *18*, 220–230.

(18) Muller, P.; Schwille, P.; Weidemann, T. PyCorrFit–generic data evaluation for fluorescence correlation spectroscopy. *Bioinformatics* **2014**, *30*, 2532–2533.

(19) Bae, W.; Yoon, T.-Y.; Jeong, C. Direct evaluation of self-quenching behavior of fluorophores at high concentrations using an evanescent field. *PLOS ONE* **2021**, *16*, e0247326.

(20) Hendrickson, W. A.; Pahler, A.; Smith, J. L.; Satow, Y.; Merritt, E. A.; Phizackerley, R. P. Crystal structure of core streptavidin determined from multiwavelength anomalous diffraction of synchrotron radiation. *Proceedings of the National Academy of Sciences* **1989**, *86*, 2190–2194.

(21) Zanetti-Domingues, L. C.; Tynan, C. J.; Rolfe, D. J.; Clarke, D. T.; Martin-Fernandez, M. Hydrophobic Fluorescent Probes Introduce Artifacts into Single Molecule Tracking Experiments Due to Non-Specific Binding. *PLoS ONE* **2013**, *8*, e74200.

(22)

(23) Zhang, L.; Perez-Romero, C.; Dostatni, N.; Fradin, C. Using FCS to accurately measure protein concentration in the presence of noise and photobleaching. **2021**, *120*, 4230–4241.

(24) Madl, J.; Weghuber, J.; Fritsch, R.; Derler, I.; Fahrner, M.; Frischauf, I.; Lackner, B.; Romanin, C.; Schütz, G. J. Resting State Orai1 Diffuses as Homotetramer in the Plasma Membrane of Live Mammalian Cells. *Journal of Biological Chemistry* **2010**, *285*, 41135–41142.

(25) Stein, J.; Stehr, F.; Schueler, P.; Blumhardt, P.; Schueder, F.; Mücksch, J.; Jungmann, R.; Schwille, P. Toward Absolute Molecular Numbers in DNA-PAINT. **2019**, *19*, 8182–8190.

Graphical TOC Entry

Some journals require a graphical entry for the Table of Contents. This should be laid out "print ready" so that the sizing of the text is correct.
Inside the `tocentry` environment, the font used is Helvetica 8 pt, as required by *Journal of the American Chemical Society*.
The surrounding frame is 9 cm by 3.5 cm, which is the maximum permitted for *Journal of the American Chemical Society* graphical table of content entries. The box will not resize if the content is too big: instead it will overflow the edge of the box.
This box and the associated title will always be printed on a separate page at the end of the document.